Three Transducers Embedded into One Single SiC Photodetector: LSP Direct Image Sensor, Optical Amplifier and Demux Device

M. Vieira[1,2,3], P. Louro[1,2], M. Fernandes[1,2], M. A. Vieira[1,2],
A. Fantoni [1,2] and J. Costa[1,2]
[1]Electronics Telecommunications and Computer Dept, ISEL, Lisbon,
[2]CTS-UNINOVA, Lisbon,
[3]DEE-FCT-UNL, Quinta da Torre, Monte da Caparica, 2829-516, Caparica,
Portugal

1. Introduction

Amorphous Si/SiC photodiodes working as photo-sensing or wavelength sensitive devices in the visible range, have been widely studied in the past for different applications (solar cells, color sensors, image sensors).

The term "amorphous" is commonly applied to non-crystalline materials prepared by deposition from gases. Research into amorphous silicon began, nearly fifty years ago (1960). At that time amorphous silicon was grown by evaporation or sputtering and exhibited a large defect density. In 1969 occurred the growth of amorphous silicon from plasma of silane by Chittiwick et al. (1969). Another research development occurred in 1975, with the demonstration of substitutional doping by Spear e LeComber (1975).

In early studies of amorphous silicon, it was determined that plasma-deposited amorphous silicon contained a significant percentage of hydrogen atoms bonded into the amorphous silicon structure. When amorphous silicon is deposited under hydrogenation conditions the hydrogen atoms binds to dangling bond defects and remove the corresponding electronic states in the band gap, which eliminates most of the trapping and recombinations centers. This process of introducing hydrogen into silicon is usually designated as passivation of the dangling bonds. These atoms were discovered to be essential to the improvement of the electronic properties of the material. Amorphous silicon is generally known as "hydrogenated amorphous silicon", or a-Si:H. Hydrogenated amorphous silicon (a-Si:H) has a sufficiently low amount of defects to be used within devices. However, the hydrogen is unfortunately associated with light induced degradation of the material, termed the Staebler-Wronski Effect (D. E. Carlson &C. R. Wronski ,1976).

Amorphous alloys of silicon and carbon (amorphous silicon carbide, also hydrogenated, a-$Si_{1-x}C_x$:H) are an interesting variant to this material. Introduction of carbon adds extra freedom for controlling the properties of the material. Increasing concentrations of carbon in the alloy widen the electronic gap between conduction and valence bands (also called "optical gap" and bandgap), in order to potentially increase the light efficiency of solar cells

made with amorphous silicon carbide layers. On the other hand, the electronic properties as a semiconductor (mainly electron mobility), are badly affected by the increasing content of carbon in the alloy, due to the increased disorder in the atomic network.

While a-Si suffers from lower electronic performance compared to c-Si, it is much more flexible in its applications. It may also produce savings on silicon material cost, as a-Si layers can be made thinner than c-Si.

One advantage is that a-Si can be deposited at very low temperatures on glass. Once deposited, a-Si can be doped in a fashion similar to c-Si, to form p-type or n-type layers and ultimately to form electronic devices.

Another advantage is that a-Si can be deposited over large areas by Plasma Enhanced Chemical Vapor Deposition (PECVD). The design of the PECVD system has great impact on the production cost of such panel, therefore most equipment suppliers put their focus on the design of PECVD for higher throughput that leads to lower manufacturing cost.

Amorphous silicon has become the material of choice for the active layer in thin-film transistors (TFTs), which are widely used in large-area electronics applications, mainly for liquid-crystal displays (LCDs).

Nowadays, modern optical networks use Arrayed Waveguide Grating (AWG) as optical wavelength (de)multiplexers (M. Bas, 2002). There has been much research on semiconductor optical amplifiers as elements for optical signal processing, wavelength conversion, clock recovery, signal demultiplexing and pattern recognition (M. J. Connelly, 2002). Here, a specific band or frequency needs to be filtered from a wide range of mixed signals. Active filter circuits can be designed to accomplish this task by combining the properties of high-pass and low-pass into a band-pass filter. Amorphous silicon carbon tandem structures, through an adequate engineering design of the multiple layers' thickness, absorption coefficient and dark conductivities (P. Louro et al., 2007) can accomplish this function.

2. Amorphous Si/SiC photosensitive devices

2.1 Device configuration and sample preparation

Voltage controlled devices, were produced by PECVD in different architectures, as displayed in Fig. 1, and tested for a proper fine tuning of the visible spectrum.

The simplest configuration is a p-i-n photodiode (#1) where the active intrinsic layer is based on an a-Si:H thin film. In the other two (#2a and #2b), the active device consists of a p-i'(a-SiC:H)-n / p-i(a-Si:H)-n heterostructures (NC5 sample code).

To test the efficiency of the internal n-p junction, a third transparent contact was deposited in-between in sample #2b. The thickness (200 nm) and the optical gap (2.1 eV) of all a-SiC:H intrinsic layers (i'-) are optimized for blue collection and red transmittance. The thickness (1000 nm) of the a-Si:H i-layers was adjusted to achieve full absorption in the green and high collection in the red spectral ranges. As a result, both front and back diodes act as optical filters confining, respectively, the blue and the red optical carriers, while the green optical carriers are absorbed across both (P. Louro et al., 2007).

The deposition conditions of the i- and i'- intrinsic layers were kept constant in all the devices. They present good optoelectronic properties with conductivities between 10^{-11} and $10^{-9}\Omega^{-1}$ cm^{-1} and photosensitivity higher than 10^4 under AM1.5 illumination (100 mW/ cm^2). To decrease the lateral currents which are crucial for device operation (P. Louro et al., 2001; M. Vieira et al., 2005), low doping levels were used and methane was added during the
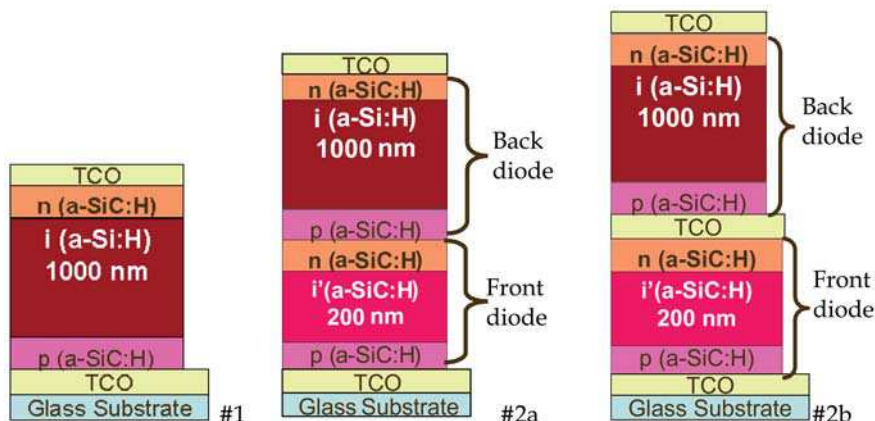
Fig. 1. Sensor element configuration.

deposition process. The doped layers (20 nm thick) have high resistivity (>$10^7\Omega$cm) and optical gaps around 2.1 eV. Transparent contacts have been deposited on front and back surfaces to allow the light to enter and leave from both sides. The back contact defines the active area of the sensor (2×2 cm^2)**.** The front and back contacts are based on ZnO:Al or ITO and have an average transmission around 80% from 425 nm to 700 nm and a resistivity around 9×10^{-4} Ωcm.

Besides, the stacked devices, the simplified test a-SiC:H p-i-n and a-Si:H p-i-n structures have also been deposited during the same deposition process. The film layers were deposited using a parallel-plate PECVD reactor. Deposition conditions such as the RF power, partial pressure and gas flow rates are shown in Table I. The substrate temperature was held at 260 °C.

Type	RF Power (W)	Pressure (mTorr)	Gas flow(sccm)			
			SiH$_4$	1% TMB+99% H$_2$	2%PH$_3$+98% H$_2$	C H$_4$
p (a-SiC:H)	4	600	10	25	–	15
i (a-SiC:H)	4	500	10	–	–	15
n (a-SiC:H)	4	500	10	–	5	15
i' (a-SiC:H)	2	400	20	–	–	–
p' (a-SiC:H)	2	400	20	10	–	–

Table I. Deposition conditions of the a-Si:H and a-SiC:H films.

2.2 Ligth-to-dark sensitivity

The typical I-V characteristics in dark and under red, blue and red&blue irradiation are displayed in Fig. 2 for the sample #1. Results show that the shape of the I-V characteristics are controlled by the background light and by the applied voltage.

To improve the light-to-dark sensitivity in sensor #1, the doped layer resistivity and optical gap were optimized. In Fig. 3 the sensitivity as a function of the wavelength is displayed under no optical bias (Φ_L=0 Wcm^{-2}) and under uniform illumination (530 nm, 2 mWcm^{-2}), respectively. Three samples were deposited keeping constant the deposition conditions for
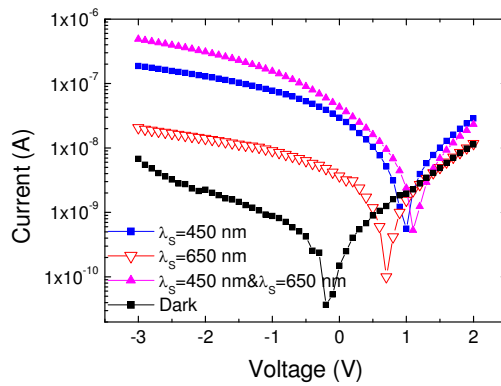
Fig. 2. I-V characteristics in dark and under red (650 nm), blue (450nm) and red&blue irradiation for the sample #1.
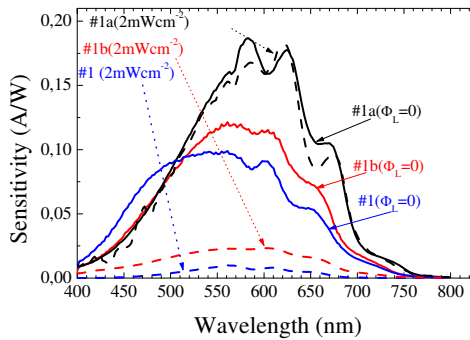

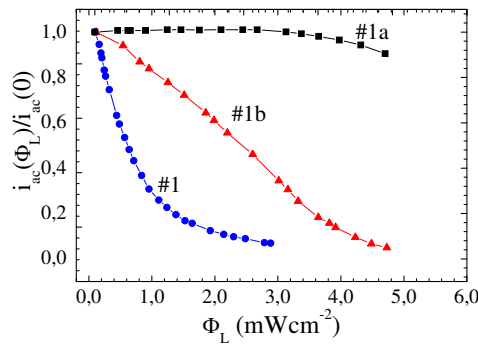Fig. 3. Spectral sensitivity with (dash) and without (solid) applied optical bias.

Fig. 4. iac(Φ_L)/iac(0) ratio dependence with Φ_L.

all i-layers, while they varied in the doped layers by adding methane during the deposition process. All the layers on sample #1a are based a-Si:H; (homostructure), while the p-layer in #1b and the p- and n-layers in #1 are based on a-SiC:H alloy (heterostructures).

Data reveals that, when wide band gap doped layers are used, the sensitivity is lower and decreases significantly with the optical bias. Under steady state irradiation the band misalignment reduces the electrical field in the bulk and increases the recombination at the interfaces decreasing the carrier collection.

In Fig. 4 we plot the light to dark sensitivity as a function of the applied optical bias, Φ_L. Results show also that the light-to-dark ratio depends strongly on the material of the doped layers. In the heterostructures the responsivity for low fluxes is high, while in the homostructure only a small signal could be detected in the flux range analyzed. When the sensor has both doped layers based on a-SiC:H layers (#1) the signal ratio steeply decreases. If only one layer is based on a-SiC:H (#1b) the signal ratio also decreases but at slower rate. Finally, in the homostructure (#1a) the sensor remains "blind" to the optical bias and only at higher light fluxes the signal ratio gently decreases. This light bias dependence enables different applications of the device depending on the readout technique. If a light scan is used to readout the generated carriers it can recognize a color pattern projected on it. If the photocurrent generated by different monochromatic pulsed channels or their combination is readout the information is multiplexed or demultiplexed and can be transmitted, tuned or recovered again.

2.3 Light filtering

The characterization of the devices was performed through the analysis of the photocurrent dependence on the applied voltage and spectral response under different optical and electrical bias conditions. The responsivity was obtained by normalizing the photocurrent to the incident flux. To suppress the *dc* components all the measurements were performed using the lock-in technique.
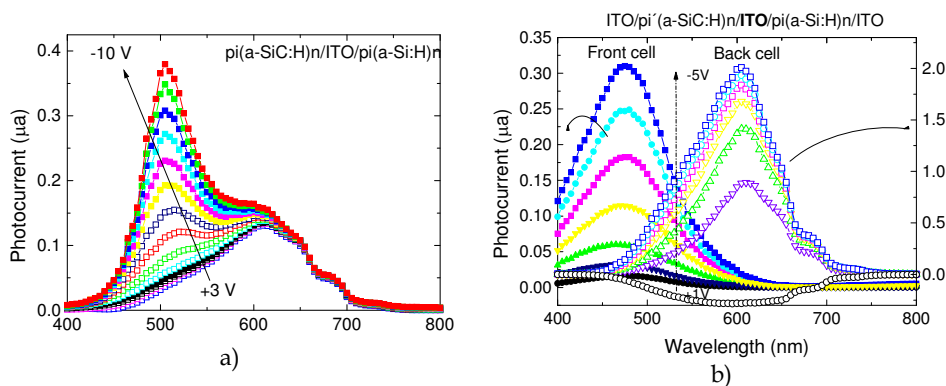

Fig. 5. a) p-i'-n-p-i-n spectral photocurrent under different applied voltages b) Front, p-i' (a-SiC:H)-n, and back, p-i (a-Si:H)-n spectral photocurrents under different applied bias.

Fig. 5a displays the spectral photocurrent of the sensor #2b under different applied bias (+3V<V<-10V), the internal transparent contact was kept floating in all measurements. In Fig. 5b the spectral photocurrent, under different electrical bias is displayed for the front, p-i' (a-SiC:H)-n, and the back p-i (a-Si:H)-n, photodiodes.

Results confirm that the front and back photodiodes act, separately, as optical filters. The front diode, based on a-SiC:H heterostructure, cuts the wavelengths higher than 550nm while the back one, based on a-Si:H, cuts the ones lower than 500nm. Each diode, separately, presents the typical responses of single p-i-n cells with intrinsic layers based on a-SiC:H or a-Si:H materials, respectively. Since the current across the device has to remain the same, in the stacked configuration, it is clearly observed the influence of both front and back diodes modulated by its serial connection through the internal n-p junction.

2.4 Optical amplification

Three monochromatic pulsed lights (input channels): red (R: 626 nm), green (G: 524 nm) and blue (B: 470nm) illuminated separately device #2a. Steady state red, green and blue optical bias was superimposed separately and the photocurrent generated measured at -8V and +1 V. In Fig. 6 the signal is displayed for each monochromatic input channel.

Results show that blue steady state optical bias amplifies the red channel and that the red light amplifies the blue channel. When an optical bias is applied it mainly enhances the field distribution within the less photo excited sub-cell: the back under blue irradiation and the front under red steady bias (see Fig. 8). So, the reinforcement of the electric field under blue irradiation and negative bias increases the collection of the carriers generated by the red channel and decrease the blue one. Under red optical bias an opposite behaviour is observed. The green bias absorption is balanced in both front and back cells. So, the green channel collection is reduced while the red and blue collections are almost insensitive to the green irradiation. This effect can be used either to amplify the red or blue channels or to tune the green one since the others remain almost constant.
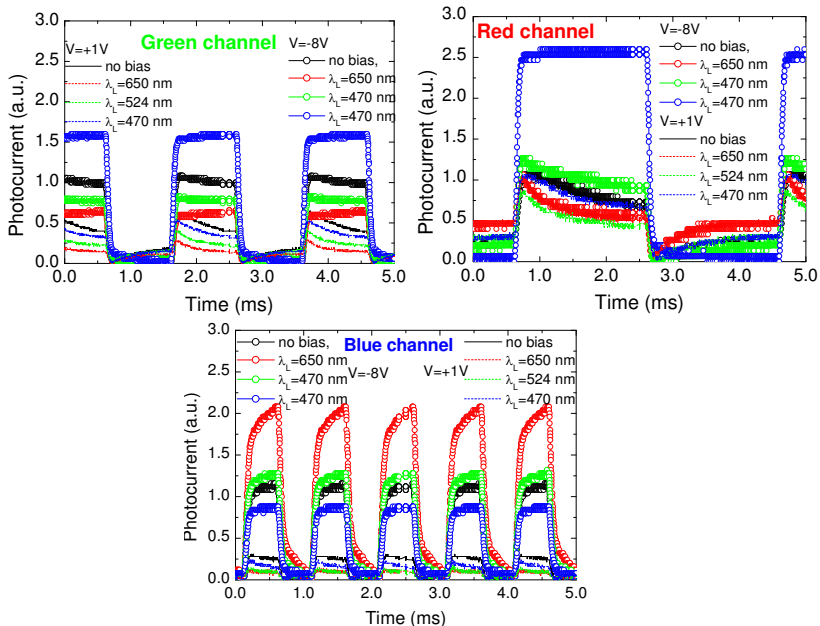

Fig. 6. Input red (a) green (b) and blue (c) signals under negative and positive bias without and with red, green and blue steady state optical bias for the #2a device.

3. Self bias effect in pinpin photodiodes

3.1 Numerical simulation

A device simulation program ASCA-2D (A. Fantoni et al., 1999) was used to analyze the potential profiles in the investigated structure. Typical values of band tail and gap state parameters for amorphous materials were used. In the films the optical band gaps were chosen in compliance with the obtained experimental values (Table I). Band discontinuities were equally distributed over the valence and conduction band offsets ($\Delta E_v = \Delta E_c = 0.15$ eV).

3.2 Generation/recombination profiles

The photogeneration/recombination profiles used in this simulation are depicted in Fig. 7 for a tandem p-i(a-SiC:H)-n/p-i(a-Si:H)-n -cell having, respectively, 200 nm and 1000 nm thick absorbers.
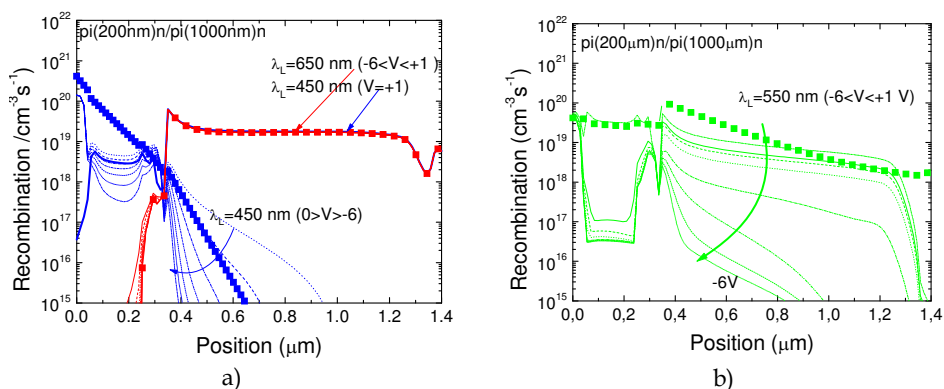

Fig. 7. Numerical simulation under different background light: (a) generation (solid lines)/recombination (dash lines) rates.

The thickness of the front diode and its optical gap was optimized for high conversion efficiency in the blue/green light and transparency of the red photons coming either from the image or from the scanner. In the a-SiC:H and a-Si:H absorbers an optical band gap of 2.1 eV and 1.8 eV and a thickness of 200 nm and 1000 nm were, respectively, chosen in compliance with the obtained experimental values for the single films. The doping level was adjusted in order to obtain approximately the same conductivity of the layers as in the tested samples.

3.3 Electrical field profiles

Fig. 8 a), b) and c) reports the simulated electric field profile within a #2-like structure under different optical bias wavelengths and for different values of the external electrical bias. In Fig. 8d) is displayed the electric field profile under thermodynamic equilibrium.

Simulated results show that the shallow penetration of the blue photons into the front diode, the deep penetration of the red photons into the back absorber or the decay of the green absorption across both, control the internal electrical field. The balance between the

electrical field adjustments due to the non uniform absorption throughout the structures depends on the generation/recombination ratio profiles at each applied voltage (Fig. 7). When an external electrical bias (forward or reverse) is applied, it mainly influences the field distribution within the less photo excited sub-cell. When compared with the electric field profile under thermo-dynamical equilibrium conditions, the field under illumination is lowered in the most absorbing cell, while the less absorbing one reacts by assuming a reverse bias configuration. Consequently, opposite behavior is observed under red and blue background light while under green light condition the redistribution of the field profile is balanced between the two sub-cells.
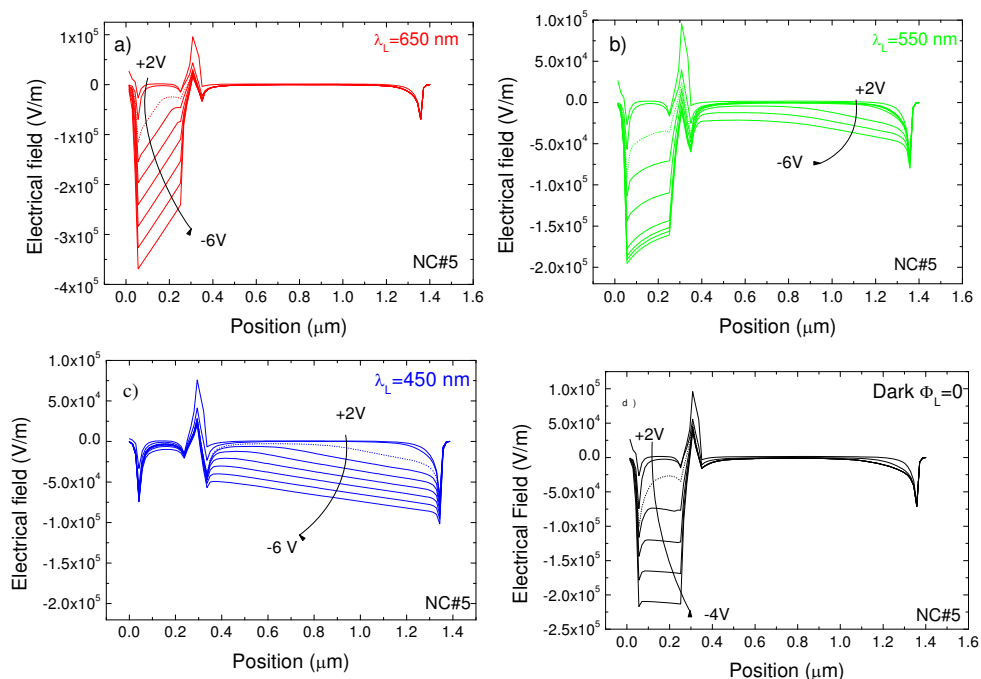

Fig. 8. Electric field profile within the p-i-n/p-i-n tandem structure for different values of the external electrical bias and for different wavelengths of impinging light: a) 650 nm; b) 550 nm; c) 450 nm d) thermodynamic equilibrium (dark) for device #2.

3.4 Potential profiles

Fig. 9 shows the simulated potential profiles at different applied voltages in dark (dash line) and under red (straight line), green (cross +) and blue (cross x) irradiation.

Results confirm that the application of an external electrical bias interferes mainly with the less absorbing cell. In the blue range as the reverse bias increases the potential drop across the non irradiated diode increases while in the front diode it remains almost negligible. In the red range the potential drop occurs across de front diode where no carriers are generated and remains negligible at the absorbing region. Due to the non uniform absorption across the back diode (Fig. 7), under green irradiation, the potential drop is

distributed across both diodes and balanced between the blue (in the back diode) and the red (in the front diode) behaviors.
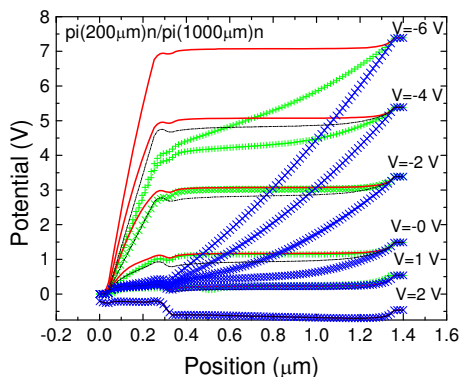

Fig. 9. Simulated potential profile under different applied voltages in dark and under red (λ_L=650 nm) green (λ_L=550 nm) and blue (λ_L=450 nm) irradiation.

3.5 Self-bias effect in p-i-n/p-i-n structures

Taking into account the geometry of the device and since light traverses through the sequence and is absorbed according to its wavelength (Fig. 7), the successive diodes should ensure that they each give the same current:

$$I_1^{pin} = I_2^{pin} = I \quad V = V_1 + V_2 \tag{1}$$

$$I_1^{pin} = I_{01}\left(\exp\left(\frac{V_1}{\eta V_T}\right) - 1\right) - I_{ph1} \quad I_2^{pin} = I_{02}\left(\exp\left(\frac{V_2}{\eta V_T}\right) - 1\right) - I_{ph2} \tag{2}$$

Where V_1 and V_2 are the voltage drop across each diode and V is the external voltage. $I_{0,1,2}$ and $I_{ph,1,2}$ are, respectively, the leakage and the photo currents, V_T the thermal voltage and η the ideality factor.

Neglecting the series resistance and assuming: $I_1 = I_{01} + I_{ph1}$ and $I_2 = I_{02} + I_{ph2}$ the current across the structure will be given by:

$$I = 0.5 \times \left(-(I_1 + I_2) + \sqrt{(I_1 - I_2)^2 + 4 I_{o1} I_{02} \exp\left(\frac{V}{\eta V_T}\right)}\right) \tag{3}$$

$$V = \eta V_T \ln\frac{(I + I_1)(I + I_2)}{I_{01} I_{02}} \quad V_1 = \eta V_T \ln\left(\frac{(I + I_1)}{I_{01}}\right) \quad V_2 = V - V_1 \tag{4}$$

Any diode whose current is bellow the other would have to reduce its bucking current and consequently voltage to try to catch up. This diode may even have to reverse bias itself in its

efforts to get in line with the other. Consequently voltage is decreased, if the diode is reverse biased, it becomes a power sink. This effect is what we call the self bias effect.

In Fig. 10 is displayed the potential across the front (V_1) and back (V_2) diodes as a function of the applied voltage (V) and for different photocurrent values. The η, I_{01} and I_{02} parameters were obtained in compliance with the experimental I-V characteristics ($I_{01} < I_{02}$).
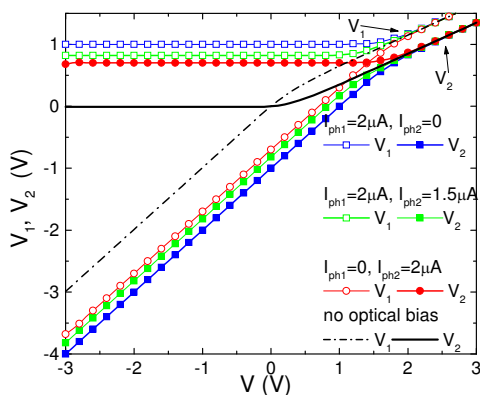

Fig. 10. Potential drop across front (V_1) and back (V_2) diodes as a function of the applied voltage (V) and for different photocurrent values.

Data show that the potential across each diode depends on the level of irradiation of both front and back diodes. Opposite behaviors are observed under red ($I_{ph1}=0$, $I_{ph2}\neq0$, Fig. 8a) and blue ($I_{ph1}\neq0$, $I_{ph2}=0$, Fig. 8c) background light. Under green ($I_{ph1}\neq0$, $I_{ph2}\neq0$, Fig. 8b) the trend depends on the I_{ph1}/I_{ph2} ratio, it approaches the blue trend if $I_{ph1}>I_{ph2}$, the red if $I_{ph1}<I_{ph2}$ and is the same as in dark if both photocurrent are balanced. Any diode whose current ($I_{1,2}^{pin}$) is below the other would have to reduce its net current (Equation 2) and consequently voltage (Equation 4) in order to try to hold up.

4. Direct LSP image and colour sensor

4.1 Colour sensitive devices

Color sensitivity in crystalline silicon video cameras is obtained by using different detection channels with three CCD arrays, or by using a mosaic of filters deposited directly onto one single solid state sensor, (R.F. Wolffenbuttel, 1987). This method can also be used for large area amorphous silicon sensor arrays and requires three sensors for each pixel. Several attempts to achieve structures capable of modifying their sensitivity spectrum by simply changing the applied bias have been reported in the literature (Y.K. Fang et al., 1987; F. Palma, 2000; M. Vieira et al., 2002). Those approaches simplify the interconnections as only two terminals are necessary.

The conventional capturing technology in an image sensor is called mosaic capture. The way that mosaic capture works is by using just one single layer of photo detectors in a mosaic pattern to capture the red, green, and blue light, or three separate layers which can absorb different wavelengths of light at different depths with each layer capturing a different color. Using three separate layers does not need to interpolate. In contrast to color

filter arrays that use light-absorbing filters, this technology converts light of all colors into useful signal information at every pixel location.

The image sensors that use the mosaic capture system have to rely on interpolation for the missing colors. Making a guess at the colors is complex which means it takes processing power. The more accurate the image sensor is, the more processing power it has to be used. Since guessing that many colors will probably never be 100% accurate, it obviously leads to color artifacts and loss of image detail.

Amorphous silicon-carbon (a-SiC:H) is a material that exhibits excellent photosensitive properties. This feature together with the strong dependence of the maximum spectral response with the applied bias has been intensively used for the development of color devices. Various structures and sequences have been suggested (H.K. Tsai & S.C. Lee, 1987; G. de Cesare, 1995; A. Zhu et al., 1998; M. Topic et al., 2000; M. Mulato et al., 2001). In our group efforts have been devoted towards the development of a new kind of color sensor. Large area hydrogenated amorphous silicon single and stacked p-i-n structures with low conductivity doped layers were proposed as color Laser Scanned Photodiode (LSP) image sensors [M. Vieira et al., 2001 ; M. Vieira et al., 2002; M. Vieira et al., 2003). These sensors are different from the other electrically scanned image sensors as they are based on only one sensing element with an opto-mechanical readout system. No pixel architecture is needed. The advantages of this approach are quite obvious like the feasibility of large area deposition and on different substrate materials (e.g. glass, polymer foil, etc.), the simplicity of the device and associated electronics, high resolution, uniformity of measurement along the sensor and the cost/simplicity of the detector. The design allows a continuous sensor without the need for pixel-level patterning, and so can take advantage of the amorphous silicon technology. It can also be integrated vertically, *i. e.* on top of a read-out electronic, which facilitates low cost large area detection systems where the signal processing can be performed by an ASIC chip underneath.

4.2 Single p-i-n laser scanned Imager

In order to analyze the light-to-dark sensitivity of sensor #1, a pattern composed by two dark regions separated by an illuminated one was projected onto the device. Then, the photocurrent (i_{ac}) generated by a low power moving spot, that scans the device in the raster mode, was measured. In Fig. 11 a line scan of the image under zero bias voltage is
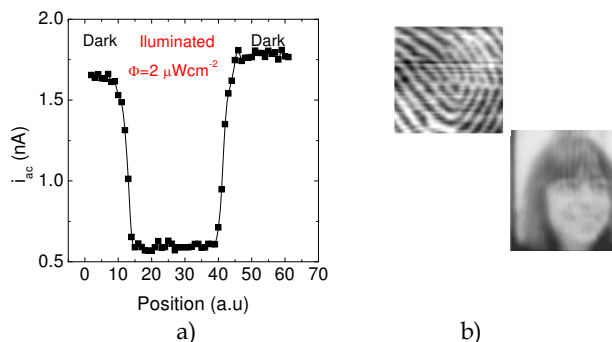

Fig. 11. a) The ac photocurrent for one dimension scan at zero bias. b) Fingerprint and grayscale photo representations.

represented. Results show that when low conductive doped layers are used the carriers are confined into the generation regions. At the illuminated regions the band misalignment reduces the electrical field in the bulk decreasing the carrier collection (low signal). In the dark regions the electrical field is high and most of the generated carriers are collected (strong signal). As a possible application, Fig. 11b displays a grayscale photo and a fingerprint representation acquired under short circuit and 10 μWcm^{-2}. No image processing algorithms were used to enhance the image. The images have good contrast and a resolution around 30 μm showing the potential of these devices for biometric applications.

4.3 Optically addressed readout

The image to acquire is optically mapped onto the photosensitive surface and a low-power light spot scans the device. The photocurrent generated by the moving spot is recorded as the image signal, and its magnitude depends on the light pattern localization and intensity.
The image and the scanner are incident on opposite sides (Fig. 12). This approach simplifies the optical system as image and scanner have different optical paths. A low power solid state red laser ($\lambda_S = 650$ nm; $\Phi_S = 10 \mu W/cm^2$) is used as scanner. The scanning beam position is controlled by a two axis deflection system. The line scan speed is close to 1 kHz. Two additional photodiodes provide the synchronization signals for the scanner position information needed for real time image reconstruction.
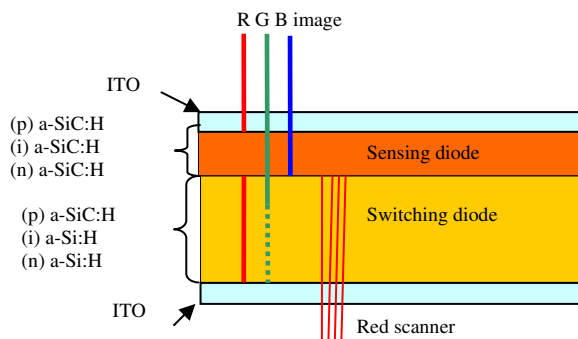

Fig. 12. Schematic of the optically addressed device optimized for colour recognition.

The current from the device is amplified and converted to digital format by a signal acquisition card installed in a computer. The data is stored as a matrix of photocurrent values (electronic image) which provide in real-time, the spatial information on the illumination conditions at the active area of the sensor (optical image). No image processing algorithms are used during the image reconstruction process.
The imaging is performed in a write-read simultaneous process: the write exposure, which converts the optical image into a localized packet of charges and the optical readout which performs the charge to current conversion by detecting the photocurrent generated by a light beam scanner. During the image acquisition process no charge transfer to move the packets of charge within the sensor is needed. This allows a real-time optically addressed readout.

4.4 Double p-i-n laser scanned colour imager

In order to optimize the readout parameters (electrical bias) and to evaluate the sensors responsivity to different light pattern wavelengths, the photocurrent generated by the scanner was measured with a lock-in amplifier under different steady-state illumination conditions bias (Φ_L=200 μWcm^{-2}, λ_L=650 nm; 550 nm; 450 nm) and displayed in Fig. 13a.
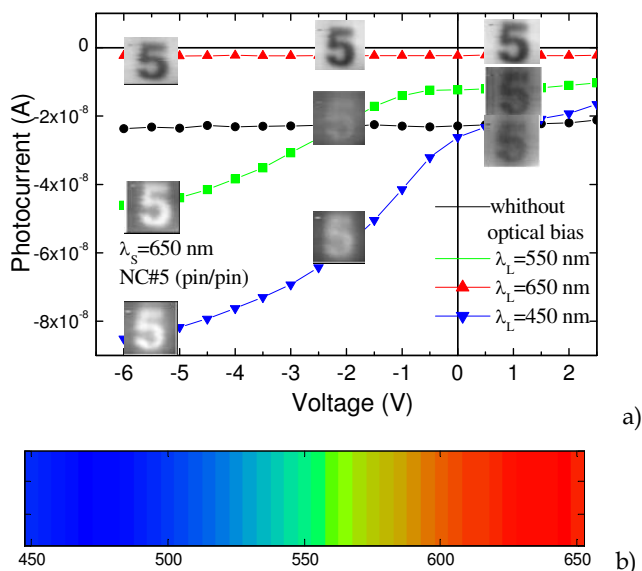

Fig. 13. a) Photocurrent as a function of the applied bias for sensors #2 in dark and under blue, green and red irradiation. (Φ_L=50μW/cm2). The inserts show, at the acquired applied voltages, the images from the same RGB picture (5). b) Digital image representation of the rainbow picture acquired with device #2a.

The images, defined as the difference between the photocurrents with and without optical bias, are shown as inserts, at the acquired applied voltages. Here the same green, red and blue pictures (**5**) were projected, one by one, onto the front diode and acquired through the back one with a moving red scanner. The line scan frequency was close to 1 kHz and no algorithms where used during the image restoration process. For a readout time of 1 ms the frame time, for a 50 lines image, is around 50 ms.

Results show that under red irradiation or in dark (without optical bias) the photocurrent generated by a red scanner is independent on the applied voltage. Under blue/green irradiation it decreases as the applied voltage changes from reverse to forward bias being higher under blue than under green irradiation. The main difference occurs in the green spectral range. It is interesting to notice that around -2 V the collection with or without green optical image is the same, leading to the rejection of the green image signal. Taking the signal without bias as a reference, and tuning the voltages to -2 V, the red and blue signal are high and opposite and the green signal suppressed allowing blue and red color recognitions. The green information is obtained under slight forward bias (+1 V), where the blue image signal goes down to zero and the red remains constant. Readout of 1000 lines per second was achieved allowing continuous and fast image sensing.

The combined integration of this information allows recording full range of colors at each location instead of just one color at each point of the captured image as occurs with the CCD image sensors. Readout of 1000 lines per second was achieved. Fig. 13b shows the digital image using as optical image a graded wavelength mask (rainbow) to simulate the visible spectrum in the range between 400 and 700 nm. For image acquisition two applied voltages were used to sample the image signal: + 1V and -6 V. The line scan frequency was close to 500 Hz. For a readout time of 2 ms the frame time for a 40 lines image takes around 80 ms. The algorithm used for image color reconstruction took into account that at -6 V the positive signals correspond to the blue/green contribution and the negative ones to the red inputs. The green information was extracted from the image signal sampled at +2 V, where the blue signal is almost suppressed and the green and red signals are negative (Fig. 13a).

4.5 Optical bias intensity and colour rejection
In order to tune correctly the applied voltage that leads to color rejection and to be sure that this value is independent on the image intensity, the photocurrent generated by the scanner (λ_S=650 nm, 10 μWcm^{-2}) was measured with a lock-in amplifier under different steady-state illumination conditions (400 nm<λ_L<750 nm, 0<Φ_L<160 μWcm^{-2}). In these measurements the element sensor was uniformly illuminated through the switching diode with red pulsed light and the different optical bias were applied through the sensing one.
In Fig. 14, for sensor #2, the scanner photocurrent dependence on the applied voltage is shown under blue (a), green (b) and red (c) optical bias and different flux irradiations (Φ_L).
Results confirm that for a wide flux range of the blue and green irradiation the amplitude of the image signal can be cancelled by tuning the applied voltage to an appropriated voltage (see arrows) allowing blue and green color rejection.

4.6 Conclusions
A wavelength-optimized optical signal and imaging device for color and image recognition is presented. A trade-off between sensor configuration (thickness and absorption coefficient of the a-SiC:H/ a-Si:H sensing switching absorbers) and readout parameters (light pattern and scanner wavelength) was established in order to improve the resolution and the contrast of the image.
When a thin a-SiC:H sensing absorber, optimized for red transmittance and blue collection, is used the detector behaves itself as a filter giving information about the radiation wavelength and the position where it is absorbed. By sampling the absorption region with three different bias voltages it was possible to extract separately the RGB integrated information with a good rejection ratio. For both sensors readout of 1000 lines per second was achieved allowing continuous and fast image sensing, and color recognition.

5. Wavelength-Division (de)Multiplexing device

5.1 DEMUX devices
Wavelength division multiplexing (WDM) devices are used when different optical signals are encoded in the same optical transmission path, in order to enhance the transmission capacity and the application flexibility of optical communication and sensor systems. Various types of available wavelength-division multiplexers and demultiplexers include prisms, interference filters, and diffraction gratings. Currently modern optical networks use
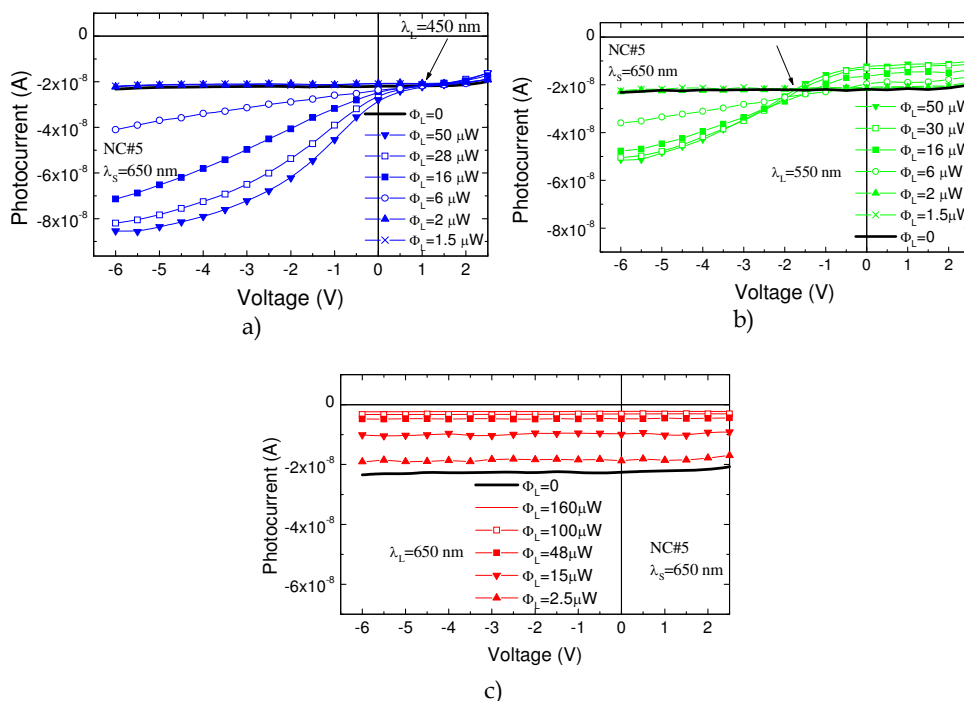
Fig. 14. Photocurrent as a function of the applied bias under blue (a), green (b) and red (c) irradiation, ($0 < \Phi_L < 160\mu W/cm^2$).

Arrayed Waveguide Grating (AWG) as optical wavelength (de)multiplexers (Michael Bas, 2002) based on multiple waveguides to carry the optical signals. In this paper we report the use of a monolithic WDM device based on an a-Si:H/a-SiC:H multilayered semiconductor heterostructure that combines the demultiplexing operation with the simultaneous photodetection of the signal. The device makes use of the fact that the optical absorption of the different wavelengths can be tuned by means of electrical bias changes or optical bias variations. This capability was obtained using adequate engineering design of the multiple layers thickness, absorption coefficient and dark conductivities (P. Louro et al, 2007, M. Vieira et al., 2005). The device described herein operates from 400 to 700 nm which makes it suitable for operation at visible wavelengths in optical communication applications.

5.2 Device operation

Monochromatic pulsed beams together or one single polychromatic beam (mixture of different wavelength) impinge in the device and are absorbed, according to their wavelength (Fig.s 5 and 7). By reading out, under appropriate electrical bias conditions, the photocurrent generated by the incoming photons, the input information is electrically multiplexed or demultiplexed.

In the multiplexing mode the device faces the modulated light incoming together (monochromatic input channels). The combined effect of the input signals is converted to an electrical signal, via the device, keeping the input information (wavelength, intensity and
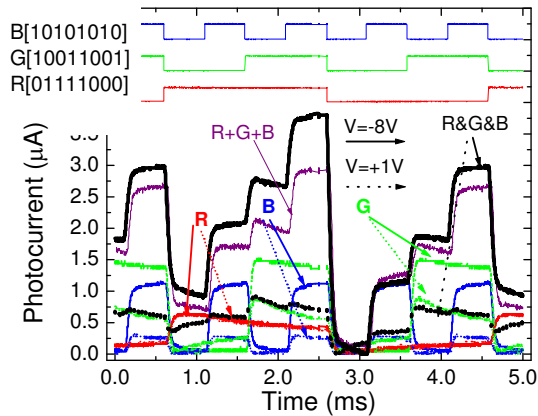
Fig. 15. Single (R, G and B) and combined (R&G&B) signals under -8V (solid arrows) and +1V (dotted arrows).

modulation frequency). The output multiplexed signal, obtained from the combination of the three optical sources, depends on both the applied voltage and on the ON-OFF state of each input optical channel. Under negative bias, the multiplexed signal presents eight separate levels. The highest level appears when all the channels are ON and the lowest if they are OFF. Furthermore, the levels ascribed to the mixture of three or two input channels are higher than the ones due to the presence of only one (R, G, B). Optical nonlinearity was detected; the sum of the input channels (R+B+G) is lower than the corresponding multiplexed signals (R&G&B). This optical amplification, mainly on the ON-ON states, suggests capacitive charging currents due to the time-varying nature of the incident lights. Under positive bias the levels were reduced to one half since the blue component of the combined spectra falls into the dark level, the red remains constant and the green component decreases.

In the demultiplexing mode a polychromatic modulated light beam is projected onto the device and the redout is performed by shifting between forward and reverse bias. Fig. 15 displays the input and multiplexed signals under negative (-8V) and positive (+1V) electrical bias. As expected, the input red signal remains constant while the blue and the green ones decrease as the voltage changes from negative to positive.

To recover the transmitted information (8 bit per wavelength channel) the multiplexed signal, during a complete cycle, was divided into eight time slots, each corresponding to one bit where the independent optical signals can be ON (1) or OFF (0). Under positive bias, the device has no sensitivity to the blue channel, so the red and green transmitted information are tuned and identified. The highest level corresponds to both channels ON (R=1, G=1), and the lowest to the OFF-OFF stage (R=0; G=0). The two levels in-between are related with the presence of only one channel ON, the red (R=1, G=0) or the green (R=0, G=1). To distinguish between these two situations and to decode the blue channel, the correspondent sub-levels, under reverse bias, have to be analyzed. The highest increase at -8V corresponds to the blue channel ON (B=1), the lowest to the ON stage of the red channel (R=1) and the intermediate one to the ON stage of the green (G=1). Using this simple key algorithm the independent red, green and blue bit sequences were decoded as: R[01111000], G[10011001]

and B[10101010], as shown on the top of Fig. 15, which are in agreement with the signals acquired for the independent channels.

5.3 Conclusion

A mulilayered device based on a-SiC:H/a-Si:H was used for demultiplexing optical signals operating in the visible range until 4000 bps. The effect of the electrical applied voltage was analyzed. A recovery algorithm to demultiplex the optical signals was proposed and tested.

6. Optical amplifier

6.1 Semiconductor amplifiers

An optical parametric amplifier comprises a material that has nonlinear, i.e., amplitude-dependent, response to each incident light wave. High optical nonlinearity makes semiconductor amplifiers attractive for all optical signals. There has been much research on semiconductor optical amplifiers as elements for optical signal processing, wavelength conversion, clock recovery, signal demultiplexing and pattern recognition (M. J. Connelly, 2002), where a particular band, or frequencies need to be filtered from a wider range of mixed signals. The basic principle of an optical amplifier is very simple. All amplifiers are current- control devices. An optical amplifier uses a changing capacitance to control the power delivered to a load. This section reports results on the use of a double pi'n/pin a-SiC:H WDM heterostructure as an active band-pass filter transfer function depending on the wavelength of the trigger light and device bias.

6.2 Steady state conditions

When an external electrical bias (positive or negative) is applied to a double pin structure, its main influence is in the field distribution within the less photo excited sub-cell (M. Vieira et al., 2008, Fig. 8). In comparison with thermodynamic equilibrium conditions (dark), the electric field under illumination is lowered in the most absorbing cell (self forward bias effect) while the less absorbing reacts by assuming a reverse bias configuration (self reverse bias effect). In Fig. 16, the spectral photocurrent at different applied voltages is displayed under red (a), green (b) and blue (c) background irradiations and without it (d).

Results confirm that a self biasing effect occurs under unbalanced photogeneration. As the applied voltages changes from positive to negative the blue background enhances the spectral sensitivity in the long wavelength range. The red bias has an opposite behavior since the spectral sensitivity is only increased in the short wavelength range. Under green background the spectral photocurrent increases with the applied voltage everywhere.

In Fig. 17 the ratio between the spectral photocurrents at +1V and -8 V, under red, green and blue steady state illumination and without it (dark), are plotted.

As expected, results show that the blue background enhances the light-to-dark sensitivity in the long wavelength range and quenches it in the short wavelength range. The red bias has an opposite behavior; it reduces the ratio in the red/green wavelength range and amplifies it in the blue one.

The sensor is a wavelength current-controlled device that make use of changes in the wavelength of the optical bias to control the power delivered to a load, acting as an optical amplifier. Its gain, defined as the ratio between the photocurrent with and without a specific background (Fig. 17) depends on the background wavelength that controls the electrical field profile across the device. If the electrical field increases locally (self optical

amplification) the collection is enhanced and the gain is higher than one. If the field is reduced (self optical quench) the collection is reduced and the gain is lower than one. This optical nonlinearity makes the transducer attractive for optical communications.
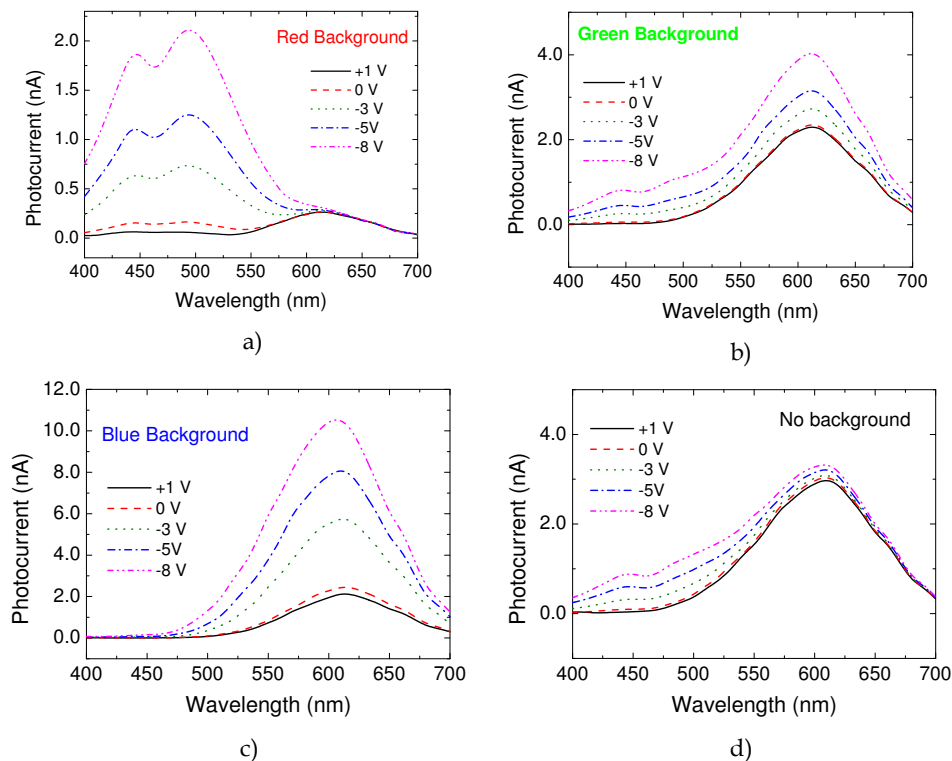

Fig. 16. Spectral photocurrent under reverse and forward bias measured without and with (λ_L) background illumination.
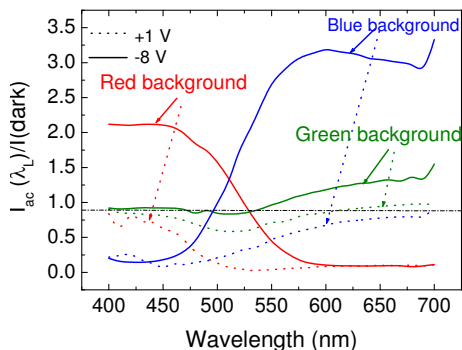

Fig. 17. Ratio between the photocurrents under red, green and blue steady state illumination and without it (no background).

6.3 Transient conditions and uniform irradiation

A chromatic time dependent wavelength combination (4000 bps) of R (λ_R=624 nm), G (λ_G=526 nm) and B (λ_B=470 nm) pulsed input channels with different bit sequences, was used to generate a multiplexed signal in the device. The output photocurrents, under positive (dot arrows) and negative (solid arrows) voltages with (colour lines) and without (dark lines) background are displayed in Fig. 18. The bit sequences are shown at the top of the figure.
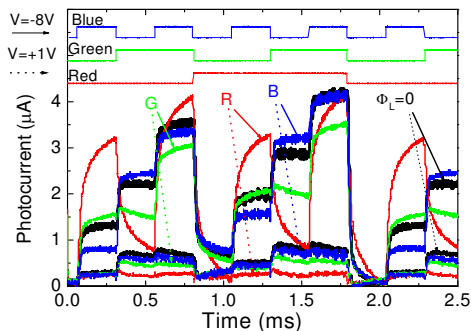
Fig. 18. Single and combined signals @-8V; without (solid arrows) and with (dotted arrows) green optical bias.
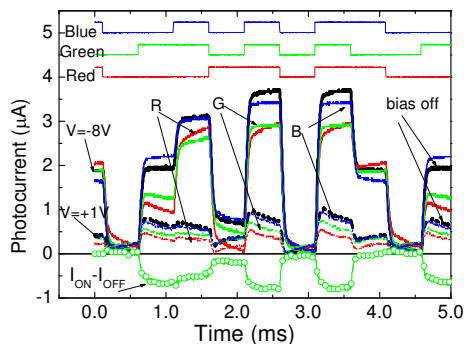

Fig. 19. Multiplexed signals @-8V/+1V (solid/dot lines); without (bias off) and with (R, G, B) green optical bias.

Results show that, even under transient input signals (from the input channels), the background wavelength controls the output signal. This nonlinearity, due to the transient asymmetrical light penetration of the input channels across the device together with the modification on the electrical field profile due to the optical bias, allows tuning an input channel without demultiplexing the stream. In Fig. 19 the green channel is tuned through the difference between the multiplexed signal with and without green bias.

7. The optoelectronic model.

7.1 Two connected transistor model

Based on the experimental results and device configuration an optoelectronic model was developed (M. A. Vieira, 2009) and displayed in Fig. 20. The optoelectronic block diagram

(a) consists of four essential elements: a double pin device for detection, a voltage supply to *dc* voltage bias; optical connections for light triggering and optical bias to *dc* light bias control. These four elements when connected together form the essentials of the optoelectronic circuit.
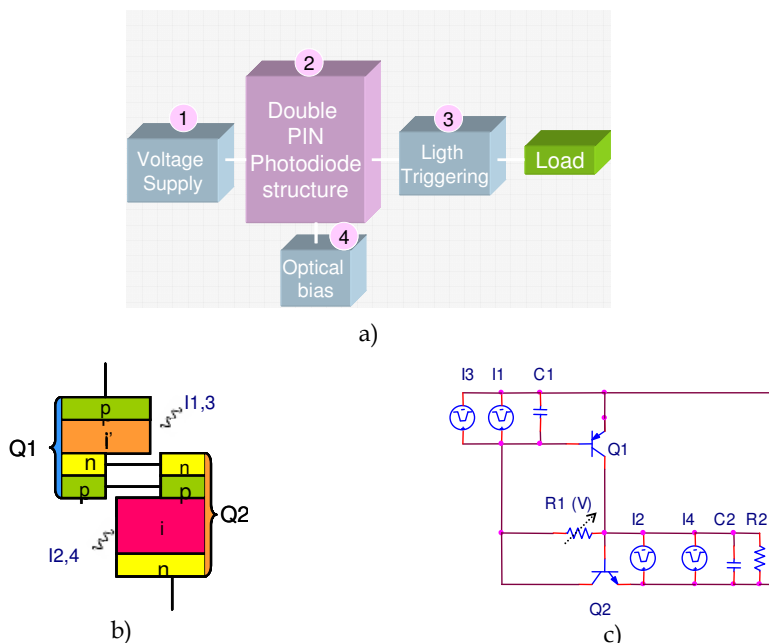

a)

b)   c)

Fig. 20. a) Optoelectronic block diagram. b) Compound connected phototransistor equivalent model. c) *ac* equivalent circuit.

The monolithic device is modelled by the two-transistor model (Q_1-Q_2) (Fig. 20b) that can be seen as a *pnp* (Q_1) and *npn* (Q_2) phototransistors separately. The *ac* circuit representation is displayed in Fig. 20c. Its operation is based upon the following principle: the flow of current through the resistor connecting the two transistor bases is proportional to the difference in the voltages across both capacitors (charge storage buckets). To trigger the device four square-wave current sources with different intensities are used; two of them, I_1 and I_2, with different frequencies to simulate the input blue and red channels and other two, I_3 and I_4, with the same frequency but different intensities to simulate the green channel due to its asymmetrical absorption across both front and back phototransistors. The charge stored in the space-charge layers is modeled by the capacitor C_1 and C_2. R_1 and R_2 model the dynamical resistances of the internal and back junctions under different *dc* bias conditions. The multiplexed signal was simulated by applying the Kirchhoff's laws for the simplified ac equivalent circuit and the four order Runge-Kutta method to solve the corresponding state equations.

Once the *ac* sources are connected in the load loop an *ac* current flows through the circuit, establishing voltage modifications across the two capacitors. During the simultaneous transmission of the three independent bit sequences, the set-up in this capacitive circuit loop is constantly changing in magnitude and direction. This means that the voltage across one capacitor builds up until a maximum and the voltage across the other builds up to a

minimum. The system then stops and builds up in the opposite direction. It tends to saturate and then leave the saturation because of the cyclic operation. This results in changes on the reactance of both capacitors. The use of separate capacitances on a single resistance R_1 results in a charging current gain proportional to the ratio between collector currents. The *dc* voltage, according to its strength, aids or opposes the *ac* currents. In Fig. 21 the simulated currents (symbols) under negative bias, with (b) and without (a) red bias, are compared. The current sources are also displayed (dash lines). To simulate the red background, current sources intensities were multiplied by the on/off ratio between the input channels with and without optical bias. The same bit sequence of Fig. 15 was used but at a lower bit rate (2000 bps). To validate the model the experimental multiplexed signals are also shown (solid lines).
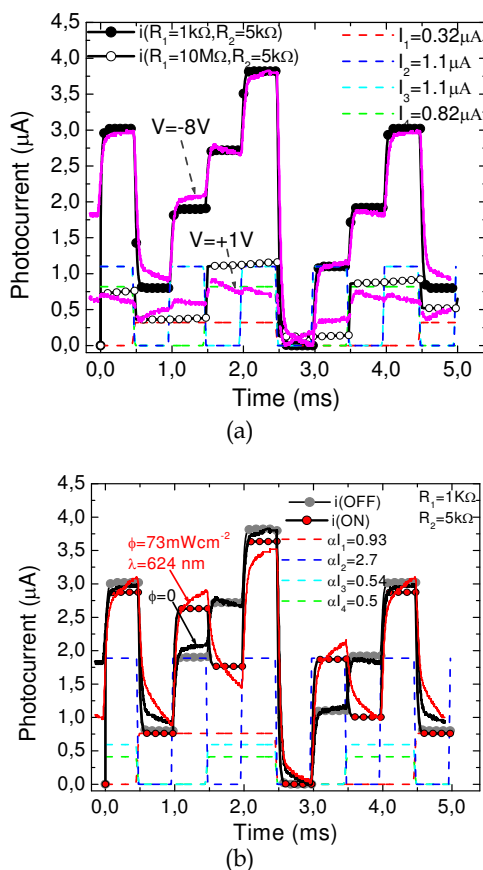

(a)

(b)

Fig. 21. Multiplexed simulated (symbols), current sources (dash lines) and experimental (solid lines): a) Positive (R_1=10MΩ; +1V) and negative dc bias. b) Negative dc bias (R_1=1kΩ; -8V) with and without red irradiation.

Good agreement between experimental and simulated data was observed. Under negative bias and if no optical bias is applied, the expected eight levels are detected, each one corresponding to the presence of three, two, one or no color channel ON. Under positive

bias or steady state irradiation the levels are amplified or reduced depending on the external control. The expected optical amplification is observed due to the effect of the active multiple-feedback filter when the back diode is light triggered.

7.2 Sensing applications

The optical amplification under transient condition also explains the use of the same device configuration in the Laser Scanned Photodiode (LSP) image and color sensor. Here, if a low power monochromatic scanner is used to readout the generated carriers the transducer recognizes a color pattern projected on it acting as a color and image sensor. Scan speeds up to 10^4 lines per second are achieved without degradation in the resolution

For the color image sensor only the red channel is used. To simulate a color image at the XY position, using the multiplexing technique, a low intensity moving red pulse scanner (Φ_S, λ_S), impinges in the device in dark or under different red, green and blue optical bias (color pattern, Φ_L, $\lambda_{RGB,L}$, $\Phi_L > \Phi_S$). Fig. 22 displays the experimental acquired electrical signals. The image signal is defined as the difference between the photocurrent with (light pattern) and without (dark) optical bias.
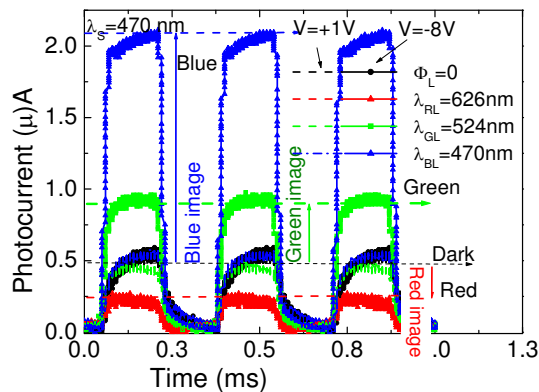

Fig. 22. Experimental color recognition using the WDM technique.

Without optical bias ($\Phi_L = 0$) and during the red pulse, only the minority carriers generated at the base of Q_2 by the scanner, flow across the circuit (I_2) either in reverse or forward bias. Under red irradiation (red pattern, $\Phi \neq 0$, λ_{RL}) the base-emitter junction of Q_2 is forward bias, the recombination increases reducing I_2 thus, a negative image is observed whatever the applied voltage. Under blue ($\Phi \neq 0$, λ_{BL}) or green ($\Phi \neq 0$, λ_{BL}) patterns irradiations the signal depends on the applied voltage and consequently, on R_1. Under negative bias, the charge transferred from C_1 to C_2, reaches the output terminal as a capacitive charging current. An optical enhancement is observed due to the amplifier action of adjacent collector junctions which are always polarized directly. Under positive bias the device remains in its non conducting state, unless the red pulse (I_2, dark level) is applied to the base of Q_2. Here, Q_2 acts as a photodiode for one polarity of the current. No amplification occurs and the red channel is strongly reduced when compared with its value under negative voltage. Under blue irradiation, the internal junction becomes reverse biased at +1 V (blue threshold) allowing the blue recognition. The behavior under a green pattern depends on the balance

between the green absorption into the front and back diodes that determines the amount of charges stored in both capacitors. Under negative bias both the green component absorbed in the front diode (blue-like) or at the back diode (red-like) reaches the output terminal while for voltages at which the internal junction n-p becomes reversed (green threshold), the blue-like component is blocked and the red-like reduced. So, by using a thin a-SiC:H front absorber optimized for blue collection and red transmittance and a back a-Si:H absorber to spatially decouple the green/red absorption, the model explains why a moving red scanner (probe beam) can be used to readout the full range of colors at each location without the use of a pixel architecture.

CCD digital image sensors are only able of recording one color at each point. Since, under steady state illumination (optical image) each phototransistor acts as a filter this multiplexing readout technique can also be used if the stack device is embedded in silicon forming a two layer image sensor that captures full color at every point. Here, a demosaicing algorithm is needed for color reconstruction.

8. Conclusions

Single and stacked pin heterojunctions based on a-SiC:H alloys were compared under different optical and electrical bias conditions using different readout techniques. Several applications is presented. A theoretical model gives insight into the physics of the device. Results show that the device can be considered as three integrated transducers in a single photodetector. If a light scan of fixed wavelength is used for readout it is possible to recognize a color pattern. On the other hand, if the photocurrent generated by different monochromatic pulsed channels or their combination is readout directly the information is multiplexed or demultiplexed. Finally, when triggered by light with appropriated wavelengths, it can amplify or suppress the generated photocurrent working as an optical amplifier. A self bias model was presented to support the sensing methodologies.

9. References

A. Fantoni, M. Vieira, R. Martins, (1999), *Mathematics and Computers in Simulation*, Vol. 49. pp. 381-401.

A. Zhu, S. Coors, B. Schneider, P. Rieve, M. Bohm, (1998) IEEE Trans. on Electron Devices, Vol. 45, No. 7, July, pp. 1393-1398.

D. E. Carlson and C. R. Wronski, (1976) *Applied Physics Letters* 33 935.

F. Palma (2000) in "Technology and Applications of Amorphous Silicon", Edited by R. A. Street, Spring-Verlag, Berlin Heidelberg New York.

G. de Cesare, F. Irrera, F. Lemmi, F. Palma, (1995) IEEE Trans. on Electron Devices, Vol. 42, No. 5, May, pp. 835-840.

H.K. Tsai, S.C. Lee, (1987) *IEEE electron device letters*, EDL-8, pp.365-367.

K.C. Chang, Chun-Yen Chang, Y.K. Fang and S.C. Jwo, (1987) "The amorphous Si/SiC heterojunctions colour-sensitive phototransistor" *IEEE electron device letters*, Vol. EDL-8,No. 2 pp.64-65.

M. A. Vieira, M. Vieira, M. Fernandes, A. Fantoni, P. Louro, M. Barata (2009), Amorphous and Polycrystalline Thin-Film Silicon Science and Technology 2009, MRS Proceedings Vol. 1153, A08-0.

M. Bas, Fiber Optics Handbook,(2002) Fiber, *Devices and Systems for Optical Comm.*, Chap, 13, Mc Graw-Hill.

M. J. Connelly (2002), *Semiconductor Optical Amplifiers*. Boston, MA: Springer-Verlag, 2002. ISBN 978-0-7923-7657-6.

M. Mulato, F. Lemmi, J. Ho, R. Lau, J. P. Lu, R. A. Street, (2001) *J. of Appl. Phys.*, Vol. 90, No. 3, pp. 1589-1599.

M. Topic, H. Stiebig, D. Knipp, F. Smole, J. Furlan, H. Wagner, (2000) *J. Non Cryst. Solids* 266-269 1178-1182.

M. Vieira, A. Fantoni, M. Fernandes, P. Louro, I. Rodrigues (2003) Mat. Res. Soc. Symp. Proc 762@2003 A.18.13.

M. Vieira, A. Fantoni, P. Louro, M. Fernandes, R. Schwarz, G. Lavareda, and C. N. Carvalho, (2008) *Vacuum*, Vol. 82, Issue 12, 8 August 2008, pp: 1512-1516.

M. Vieira, M. Fernandes, A. Fantoni, P. Louro, and R. Schwarz, (2002) "A new CLSP sensor for Image recognition and color separation", Mat. Res. Soc. Symp. Proc., Editors: Cohen, Abelson, Matsumura, Robertson, 715 (2002) pp.695-700.

M. Vieira, M. Fernandes, J. Martins, P. Louro, R. Schwarz, M. Schubert, (2001) *IEEE Sensor Journal*, 1, no.2 (August) pp. 158-167.

M. Vieira, M. Fernandes, P. Louro, R. Schwarz, M. Schubert (2002), *J. Non Cryst. Solids* 299-302 pp.1245-1249.

Michael Bas (2002), *Fiber Optics Handbook, Fiber, Devices and Systems for Optical Communication*, Chap, 13, Mc Graw-Hill, Inc. 2002.

P. Louro, M. Vieira, Yu. Vygranenko, A. Fantoni, M. Fernandes, G. Lavareda, N. Carvalho (2007) Mat. Res. Soc. Symp. Proc., 989, A12.04.

P. Louro, M. Vieira, Yu. Vygranenko, M. Fernandes, R. Schwarz, M. Schubert (2001), *Applied Surface Science* 184, 144-149 (2001).

R.C. Chittick, J.H. Alexander, H. F. Sterling, (1969) *J. Electrochem. Soc*. 116, 77 .

R.F. Wolffenbuttel, (1987) "Color filters integrated with he detector in silicon" *IEEE electron device letters*, Vol. EDL-8,No. 1 (1987) pp.13-15.

W. E. Spear and P. G. Le Comber (1975), *Solid State Commum*. 17, 1193 (1975)

Y.K. Fang, S.B. Hwang, Y.W. Chen, and L.C. Kuo, (1987) "vertical type a-Si:H back-to-back Schottky diode for high-seed colour image sensor" *IEEE electron device letters*, Vol. EDL-8,No. 2 pp.64-65.
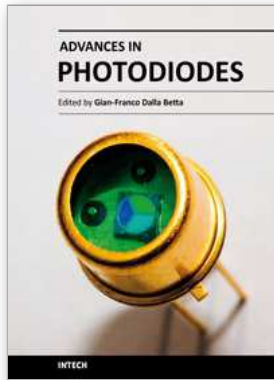
Advances in Photodiodes

Edited by Prof. Gian Franco Dalla Betta

Photodiodes, the simplest but most versatile optoelectronic devices, are currently used in a variety of applications, including vision systems, optical interconnects, optical storage systems, photometry, particle physics, medical imaging, etc. Advances in Photodiodes addresses the state-of-the-art, latest developments and new trends in the field, covering theoretical aspects, design and simulation issues, processing techniques, experimental results, and applications. Written by internationally renowned experts, with contributions from universities, research institutes and industries, the book is a valuable reference tool for students, scientists, engineers, and researchers.

How to reference

In order to correctly reference this scholarly work, feel free to copy and paste the following:

M. Vieira, P. Louro, M. Fernandes, M. A. Vieira, A. Fantoni and J. Costa (2011). Three Transducers Embedded into One Single SiC Photodetector: LSP Direct Image Sensor, Optical Amplifier and Demux Device, Advances in Photodiodes, Prof. Gian Franco Dalla Betta (Ed.), ISBN: 978-953-307-163-3, InTech, Available from: http://www.intechopen.com/books/advances-in-photodiodes/three-transducers-embedded-into-one-single-sic-photodetector-lsp-direct-image-sensor-optical-amplifi

INTECH
open science | open minds